Laser-Induced AuNPs/ZnO-NWs/MoS_2-NSs-Coated TTIT-Shaped Seven-Core Fiber-Based Biosensor for Riboflavin Detection

Ziyi Liu, Ragini Singh, Guoju Wang, Guoru Li, Bingyuan Zhang, and Santosh Kumar, *Senior Member, IEEE*

***Abstract*—Riboflavin (RF) is an important vitamin necessary for human living activities. It is a crucial component of the body's critical enzymes, contributing to energy production, development, and metabolism. Low-cost RF sensors are one of the most essential research objectives for today's development. In this work, the authors developed a highly sensitive optical platform for real-time detection of RF concentration, with the goal of developing and testing a novel RF sensor based on localized surface plasmon resonance (LSPR) with a tri-tapered-in-tapered (TTIT) seven-core fiber with multimode structure for fast and selective RF concentration measurement in solution. In this work, a TTIT fiber-based RF sensor was developed using a fusion splicer and tapered fiber optic fabrication techniques, in which gold nanoparticles (AuNPs), zinc oxide nanowires (ZnO-NWs), and molybdenum disulfide nanosheets (MoS_2-NSs) were uniformly coated on the surface of the optical fiber to enhance the evanescent field in the sensing region, reducing optical signal loss and increasing the sensing area. To detect changes in RF concentration, the evanescent field can stimulate the LSPR of AuNPs immobilized on the probe surfaces. Furthermore, the sensor has great repeatability and stability, and the RF fiber-optic sensor developed in this experiment is an efficient, sensitive, and cost-effective mode of detection for rapid monitoring of RF levels in a wide range of practical applications. The sensor's sensitivity was 2.14 nm/mM, with a limit of detection (LOD) of 86.86 μM. The success of the technique will encourage the development of RF detection technologies for food safety and clinical diagnosis.**

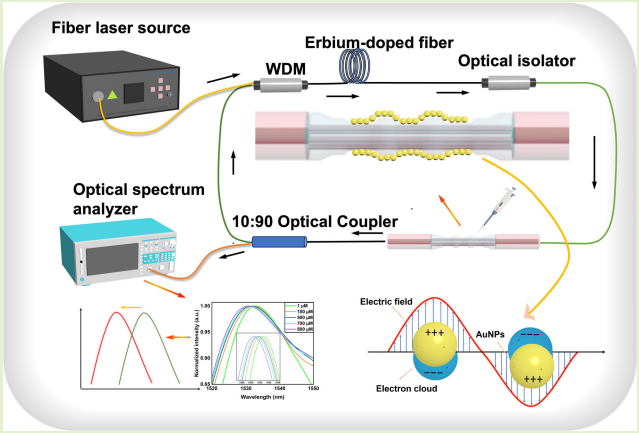

***Index Terms*—Gold nanoparticles, localized surface plasmon resonance (LSPR), multicore fiber, optical fiber sensor, Riboflavin (RF).**

I. Introduction

RIBOFLAVIN (RF), also known as vitamin B2, is a water-soluble vitamin produced by all plants and most microorganisms and is essential for the survival of both humans and animals. RF participates in redox reactions in all organisms as a coenzyme, and has therapeutic potential for oxidative stress states [1]. In addition, the recommended dietary allowances for human and animal nutrition are 0.4–0.6 mg/day and 0–17.5 mg/kg of RF [2]. The main role of RF in the human body is to aid in the proper functioning of the body [3], especially in energy production and red blood cell formation. RF plays an important role in the body as an essential vitamin, but it cannot be synthesized in the body and can only be obtained from dietary sources including cheese, tea, alcohol, and eggs. Deficiency of RF affects the biological aging of the body, causing metabolic disorders and leading to health problems. If the body is deficient in RF, symptoms such as slow growth, easy fatigue, slow metabolism, and mouth ulcers may occur. RF can also be used to prevent migraines

Manuscript received 3 May 2024; revised 26 June 2024; accepted 27 June 2024. Date of publication 9 July 2024; date of current version 15 August 2024. This work was supported in part by Liaocheng University under Grant 318052341, in part by the Special Construction Project Fund for Shandong Province Taishan Mountain Scholars, and in part by the Science and Technology Support Plan for Youth Innovation of Colleges and Universities of Shandong Province of China under Grant 2022KJ107. The associate editor coordinating the review of this article and approving it for publication was Dr. Ing. Emiliano Schena. *(Corresponding authors: Bingyuan Zhang; Santosh Kumar.)*

Please see the Acknowledgment section of this article for the author affiliations.

Digital Object Identifier 10.1109/JSEN.2024.3421325

and to treat hereditary diseases [4]. Impaired RF balance in humans can lead to multisystem dysfunction, including neuromuscular diseases, anemia, fetal developmental abnormalities, and cardiovascular diseases [5], and the health status of the body can be determined by measuring the level of RF in the body. RF is an important coenzyme in photosynthesis, which promotes the growth and development of plants, and it is one of the nutrients necessary for the growth of seafood, which is essential for the maintenance of normal life activities of the human body, as well as the growth of plants and animals. RF is very important for maintaining the normal life activities of the human body and the cultivation of plants and animals. RF is also used to determine whether food is out of date due to its excellent photosensitivity, and it is also used to treat inflammation, angina, and other diseases due to the pharmacological properties of RF, so the importance of establishing a fast and sensitive RF sensor is self-evident.

The methods currently used to detect RF concentration include electrochemical detection [6], capillary electrophoresis [7], colorimetric detection [8], high-performance liquid chromatography (HPLC) [9], fluorescence detection [10], and mass spectrometry [11]. However, all of them have their own limitations, such as high cost, weak anti-interference ability, ease of contamination, etc. However, more and more attention has been paid to the role played by RF in human life, to promote the development of RF sensors, this work develops an RF fiber optic sensor based on localized surface plasmon resonance (LSPR), which is based on the fiber optic structure of multimode fiber (MMF)- seven core fiber (SCF)-MMF. This work constructs a highly sensitive optical system for real-time detection of RF concentration in a more portable way, which has real-time, miniaturization and sensitivity.

Nanomaterials (NMs) are rapidly developing, the main properties of NMs depend on their precise composition, size, and shape. The smaller NMs are highly biocompatible and suitable for the detection of small biomolecules at low concentrations and also provide more possibilities for the construction of functionalized structures [12]. The advancement of modern technology has allowed scientific research to have powerful characterization and synthesis tools, which have made the sizes of the generated NMs more controllable [13]. The development of NMs has also promoted the development of sensors. For example, fiber optic sensors based on the LSPR phenomenon. The most commonly used NMs for such sensors are AuNPs and AgNPs. AuNPs are chosen because of their unique physicochemical properties, low cytotoxicity, and optical properties of AuNPs, and due to the large surface area of AuNPs, the chemical functional groups can be immobilized on the surface of the gold [14]. The formation of stable chemical bonding of AuNPs with S- and N-containing groups makes AuNPs firmly immobilized on the surface of optical fiber possible. The modification of other NMs in turn endowed AuNPs with excellent biocompatibility [15]. Zinc oxide nanowires (ZnO-NWs) have excellent optical transparency, biocompatibility, easy accessibility for synthesis, and their forest-like structure can capture light signals in optical fibers, reduce light loss, and increase the area of the sensing zone [16], improving the sensing performance of the sensor. Molybdenum disulfide nanosheets (MoS_2-NSs) are based on layered transition metal sulfur compounds, which have received widespread attention because of their superior electrical and optical properties. MoS_2 has a high sensitivity that can quickly find the changes in the external environment. It has also high electrical conductivity, a large specific surface area, and a strong van der Waals force that can be well fixed on the surface of the optical fiber, and it can provide a wide range of adhesion sites for other materials [17].

In recent years, the rapid development of sensors has contributed to the progress of human life. Zhang et al. [18] reviewed LSPR fiber optic sensors, including the principle, structure, and application in biosensors, etc. It introduced the fiber optic sensors with different structures in detail and also made a future outlook of the fiber optic biosensors based on LSPR. The current goal of the sensor is to continuously improve the sensitivity and limit of detection (LOD), and in the near future, the sensor will go out of the laboratory and enter into various fields of human life.

Zhu et al. [19] proposed a tapered fiber based on LSPR to detect the concentration of ascorbic acid. Goicoechea et al. [20] proposed a fiber optic sensor based on the LSPR phenomenon of AgNPs and AuNPs for detecting the concentration of H_2O_2. In this, AgNPs in the presence of H_2O_2 oxidation occur which reduces the efficiency of plasma coupling, and the concentration of H_2O_2 is analyzed based on the spectral response.

In this work, a new type of RF fiber optic sensor based on LSPR with a tri-tapered-in-tapered (TTIT) structure is proposed. The TTIT structure makes the transmission of optical signals in the probe more complex, repeatedly breaking the original optical signal transmission mode. The AuNPs, ZnO-NWs, and MoS_2-NSs are uniformly coated on the surface of the optical fiber in sequence, to stimulate the phenomenon of LSPR, which endows the sensor with high sensitivity and excellent optical coupling. The sensor has high sensitivity and excellent sensing performance.

In this work, a real-time continuous, label-free, and highly sensitive optical detection platform was built. In this experimental setup, a laser light source was used. The laser light source has the advantages of strong anti-interference ability, high stability, and fast response time. This work uses erbium-doped fiber (EDF) as the gain medium, EDF operates around 1530 nm, its fiber loss ratio is low, and has great application value. The wavelength range for interrogation of this work is near infrared (NIR). Visible lasers have less penetration depth compared to mid-infrared lasers and NIR lasers. Ultraviolet laser is too high energy interaction with biological tissues. NIR light is able to penetrate certain materials, including human tissue, more efficiently than visible light, making it invaluable in applications such as medical imaging. An EDF was utilized as a gain medium, which served as a signal amplifier and improved the sensitivity of the sensor.

The developed sensor showed good stability, reproducibility, reusability, and stability in various tests. The developed sensor has a sensitivity of 2.14 nm/mM and a LOD of 86.86 μM.

The experimental results show that the developed sensor can further promote the development of RF concentration detection technology.

II. Experimental Section

A. Materials

Acetone, hydrogen peroxide solution (H_2O_2, 30%), concentrated sulfuric acid (H_2SO_4, 98%), deionized water (DI), (3-mercaptopropyl) trimethoxysilane (MPTMS), and ethanol were used for the cleaning of the probe surfaces and the immobilization of the AuNPs. AuNPs solution was synthesized with chloroauric acid ($HAuCl_4$), trisodium citrate (sodium citrate), and deionized water (DI water). Further, the probes were immobilized with ZnO-NWs and MoS_2-NSs.

B. Instruments

A fiber optic cutter (CT-32, Fujikura) was used to cut the stripped coated fiber to obtain a flat end face, the fiber was cut to the appropriate length. Then a fiber optic fusion splicer (FSM-100P+, Fujikura, Japan) was used for fusion splicing of hetero-core fibers, and finally, a fiber optic combiner manufacturing system (CMS, USA) was used for fiber optic taper pulling. The above steps were used to fabricate the MMF-MCF-MMF-based TTIT sensing probe. The absorption spectra of the AuNPs were measured with a UV-visible spectrophotometer (Hitachi-U-3310) to determine the morphology of the AuNPs. The micro-distribution of the NMs in the solution to be tested was observed using a high-resolution transmission electron microscope (HR-TEM, Talos L120C, Thermo Fisher Scientific, USA). The spectra of the solutions to be tested were measured by an optical spectrum analyzer (OSA, AQ6370D, Yokogawa Electric) to study the optical properties of the developed sensing probes.

C. Sensing Mechanism of the Probe

When the incident light is transmitted from the high refractive index (RI) medium to the low RI medium, the total internal reflection phenomenon occurs, and evanescent fields (EWs) are generated on the side of the cladding medium. Sensors based on the LSPR phenomenon have excellent sensing performance on the premise of generating strong EWs, which interact with the AuNPs whose sizes are smaller than the wavelength of the incident light. The frequency of the EWs is in line with the oscillation frequency of free electrons of the AuNPs, and it is excited, then LSPR generation. Powerful EWs can effectively excite the LSPR to produce absorption peaks associated with RI, and can also overlap sufficiently with the liquid to be measured to sense the concentration of the liquid to be measured. To make optical fibers produce powerful EWs to excite the generation of LSPR phenomenon to enhance the high sensitivity of the probe and its sensing properties, modern optical fiber fabrication technology methods are commonly used. In this work, the pull-taper technique and core mismatch are used, where the pull-taper makes the fiber optic bent compared to the conventional fiber structure. The diameter of the core-cladding of a tapered optical fiber (TOF) gradually becomes smaller, changing the original light propagation mode, with a larger mode field, a wider spectral range, and generating more powerful EWs. In this work, the use of the TTIT structure changes the nature of the waveguide modes by altering the waveguide geometry, and it can be regarded as a kind of multimode interferometer. In TTIT, a portion of the light will penetrate the layer for several wavelength distances with a tendency of gradual attenuation, and this distance is the depth of penetration (d_p), which can be expressed by the equation

$$d_p = \frac{\lambda_i}{2\pi\sqrt{n_{\text{co}}^2 \left(\sin\theta_i\right)^2 - n_{\text{cl}}^2}} \tag{1}$$

where θ is the angle of incidence of light between the fiber's core and cladding surfaces, λ is the wavelength of the incoming light, and n_{co} and n_{cl} are the RIs of the core and cladding, respectively. The fiber outer membrane in the environment RI shifts, the incidence angle of the light signal will alter, hence altering the light's phase difference, the optical field inside the fiber coupling and reorganization, and the transfer function is

$$I = I_1 + I_2 + \sqrt{I_1 I_2 \cos\left(\Delta\varphi\right)} \tag{2}$$

where I_1 is the optical power of the inner membrane of the core and I_2 is the optical power of the cladding mode, where $\Delta\varphi = (2\pi/\lambda\ \Delta nL)$ is the phase difference, where L and λ are the interaction length and the input wavelength, respectively, and $\Delta n = n\text{eff}_1 - n\text{eff}_2$ is the difference in the modal effective indices between the inner membrane of the core and the cladding mode.

The LSPR spectral peak wavelength (λ_m) is given by

$$\lambda_m = \lambda_p\sqrt{2n_m^2 + 1}. \tag{3}$$

The wavelength (λ_p) corresponds to the frequency of the AuNPs, while n_m represents the RI of the surroundings. For AuNPs with well-defined sizes and shapes, the change of the resonance wavelength ($\Delta\lambda$) in the LSPR spectra can be written as follows:

$$\Delta\lambda = g\Delta n\left[1 - e^{-\frac{2t}{d_p}}\right] \tag{4}$$

where g is the response of AuNPs to RI, t is the thickness of the effective adsorption layer, and Δn is the change in relative RI of the surrounding environment.

D. Fabrication of Sensor Probe

A fiber optic fabrication based on the LSPR sensor structure as a TTIT structure for detecting RF is shown in Fig. 1. In this work, an SCF (6.1/125 μm) and an MMF (62.5/125 μm) were used to prepare the sensing probe. SCF has seven cores, low loss when fused to MMF, and high sensitivity to changes in RI. Because of its many unique advantages, SCF can be used to make the sensing probe for this work. Compared to other optical fibers, SCF have multiple cores within their cladding, which enhances the freedom of fiber parameters and the possibility of manufacturing sensors by fusion splicing with MMF.

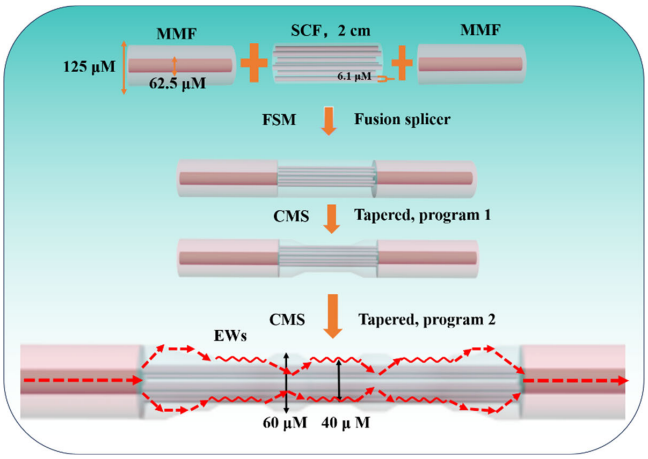

Fig. 1. Fabrication procedures and mode-coupling phenomena inside of TTIT structure.

The internal structure of the fiber optic fusion splicer machine (FSM-100+, Fujimura) is shown in Fig. 2(a), where the optical fiber was fusion spliced with the FSM to get the structure of MMF-SCF-MMF, and then the optical fiber was fabricated by pulling the fiber with the CMS. Firstly, the coating layer of a certain length of SCF and MMF was removed with a fiber stripper, the fiber was cut flat with a fiber cutter, and the MMF and SCF were placed at both ends of the FSM electrodes and fusion spliced to obtain the MMF-SCF, and the length of SCF was left at 2 cm with a fiber cutter. In the same procedure, the MMF-SCF was fusion spliced with the MMF to obtain the MMF-SCF-MMF structure of the fiber, and then the fiber was tapered with CMS. CMS uses 3SAE's thermally stabilized plasma technology to heat the fiber. The plasma has a high thermal stability and is more advanced than traditional arc heating. Fig. 2(b) shows the main internal structure of the CMS. The CMS requires preset parameters and platform calibration prior to use, and calibration of the stretching platform reduces errors due to differences in fiber positions. A single taper is pulled in the SCM region of the previously obtained fiber, and then a program is used to construct a triple taper structure based on the single taper, which results in the TTIT.

E. Synthesis Process of AuNPs/ZnO-NWs/MoS_2-NSs

Turkevich method was used to synthesize AuNPs with a diameter of 10 nm [21]. $HAuCl_4$ was used as the precursor and trisodium citrate as the reducing agent. First, $HAuCl_4$ was dissolved in DI water, and then this solution was stirred with a magnetic stirrer and brought to an ebullition at 100 °C. At this moment, the trisodium citrate solution was poured immediately. Afterward, heating and stirring were continued for 5 min and the color of the solution changed to burgundy. Stirring was continued for 10 min to obtain a homogeneous solution of AuNPs and the stirring was turned off. The ZnO-NWs were dissolved in DI water and then sonicated for two hours then ZnO-NWs solution was obtained. 30 mg of MoS_2-NSs was added to 20 mL of NMP. It was sonicated in an ultrasonic bath sonicator for 3 h, followed by sonication for 10 min at an output power of 125 w at 25 °C. The tip was pulsed to on mode (7 s) and off mode (5 s) to avoid overheating effects. The

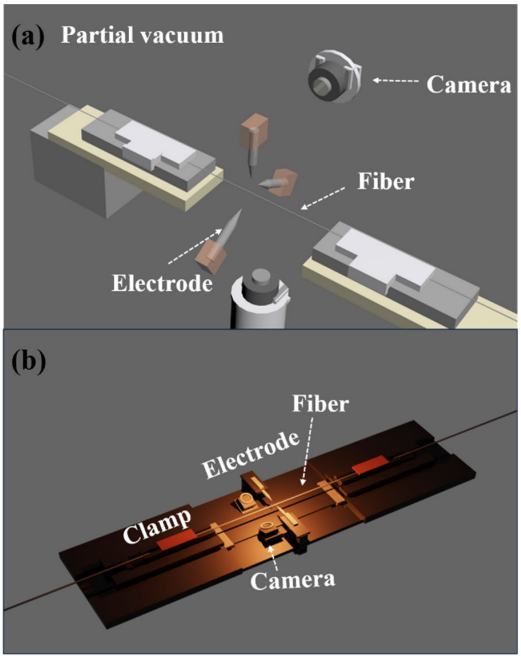

Fig. 2. Schematic of the internal of (a) CMS and (b) FSM.

MoS_2-nanosheets were further dispersed. The dispersion was again centrifuged at 5500 r/min for 1 h at 10 °C. One-third of the supernatant was collected to obtain MoS_2-NSs solution.

F. Nanocoating Immobilization

The fiber optic probe was first cleaned by immersing it in acetone solution for 20 min, then deionized water was used to make the surface of the probe smooth. Then, the probe was further cleaned by immersing it in a mixture of the solution (30% H_2O_2: concentrated H_2SO_4 = 3:7) for 30 min, then the fiber was thoroughly cleaned with deionized water. Then, the fiber was dried in an oven at 70 °C for 20 min, and then the probe was immersed in a 1% ethanol MPTMS solution for 12 h, taking care to consider the liquid sealing. MPTMS will be used as a coupling reagent to promote the adhesion of AuNPs to the surface of the optical fiber, followed by drying in ethanol and then nitrogen gas, and then the optical fiber probe was immersed in the AuNPs solution for 48 h. The probe was then rinsed with ethanol and dried with nitrogen gas to remove the unbounded AuNPs. The optical fiber was immersed in 10 mL of ZnO-NWs solution for 10 min and dried in an oven at 70 °C. This process was repeated three times to ensure that the ZnO-NWs layer was uniformly covered on the surface of the probe and to improve the stability of the ZnO-NWs immobilized probe. The same procedure was used to immobilize the MoS_2-NSs solution. Finally, the fiber optic probe with uniform AuNPs, ZnO-NWs, and MoS_2-NSs distribution layer was obtained, and the whole immobilization process is shown in Fig. 3.

G. Preparation of RF Solutions

In this work, LSPR spectra of five RF sample solutions of known concentration were measured. A 10 mL stock solution was prepared by dissolving 3.8 mg of RF in 10 mL of 1X PBS.

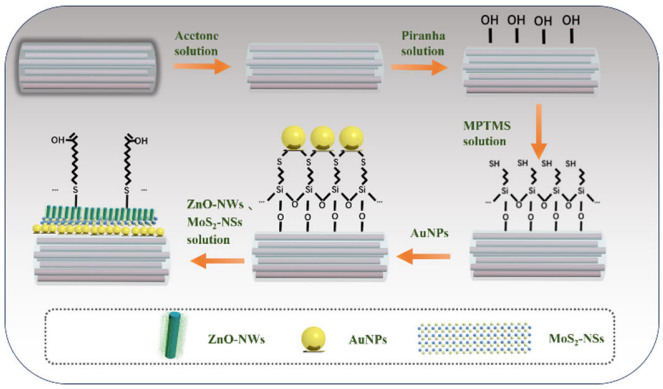

Fig. 3. Process of NMs immobilization over the optical fiber structure.

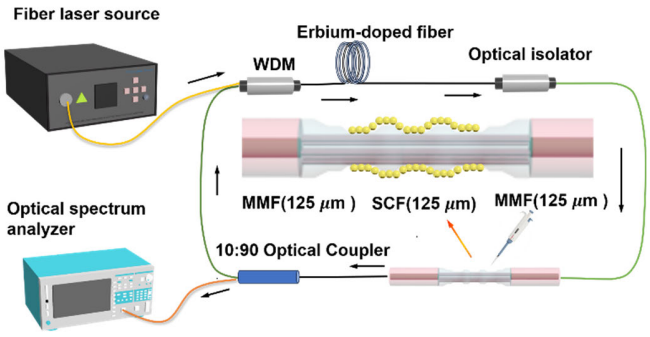

Fig. 4. Experimental setup for Riboflavin measurement.

Then different concentrations of RF solutions were made sequentially by diluting the stock solution at concentrations of 1, 100, 500, 700, and 800 μM. The amount of change in the concentration of RF was obtained by calculating the offset of the resonance peaks of the LSPR spectra. The specific steps for measuring the spectra were as follows: the probe was placed in the reaction cell and fixed with a jig, then RF solution was dropped around the probe with a pipette gun, and the spectral images and data were recorded after ten minutes.

H. Experimental Setup

The schematic of the experimental setup is shown in Fig. 4. The optical signal is generated by a pump laser source (947 nm, Max-ray Photonics Company Ltd.), the optical spectrum analyzer (OSA, 600–1700 nm), and the experimental setup consists of a 2 m-long highly EDF (ER12-6, Fibercore) with absorption of 12 dB/m at 915 nm, an optical signal isolator to prevent reflected light from affecting the stability of the system, and a wavelength division multiplexer (WDM) coupler to couple the power into the cavity. The EDF was used as a gain medium to achieve the amplification of the optical signal, which can improve the sensitivity of the sensor. The developed probe is inserted into the annular cavity along with a 10:90 coupler, 10% of the coupler output transmits the laser output signal, which can be observed by the OSA, and 90% feeds into the cavity, which creates an annular cavity. When the optical signal passes through the probe, the strong and effective EWs excite the LSPR phenomenon of AuNPs. When the optical signal passes through the probe, the change of the concentration of the substance to be measured around the probe causes the change of the EWs, which makes it possible to measure the drift of the LSPR resonance spectral peak of the substance to be measured and transform the amount of the peak drift into the amount of the change of the concentration of the substance to be measured. Different concentrations of the RF solution are analyzed based on the LSPR spectrum of the RF solution, and when the spectral output is stable, data corresponding to each concentration are recorded.

III. Results and Discussion

A. Optimization of Optical Fiber Sensor Probe

In the manufacture of optical fibers, the fiber fusion process of FSM and the fiber tapering process of CMS are used. The use of a modern advanced optical fiber modification process makes the traditional optical fibers produce effective and powerful EWs, which can stimulate the LSPR phenomenon more effectively, and the detection of RF concentration is more sensitive and accurate. The most important aspect of using FSM and CMS is to determine the parameters of fiber optic manufacturing. It needs to be adjusted repeatedly to make the manufactured fiber optic probes highly sensitive and highly repeatable.

B. Characterization of NMs

The peak of the absorption spectrum of AuNPs is at 519 nm, as measured by a UV-visible spectrophotometer and plotted in Fig. 5(a). It indicates that the synthesized AuNPs have a diameter of about 10 nm and are capable of better excitation of the LSPR phenomenon. The morphology and distribution of the NMs were examined by HR-TEM. It revealed that the synthesized AuNPs are spherical and uniformly dispersed. Meanwhile, HR-TEM was used to characterize the microscopic morphology of the ZnO-NWs and MoS_2-NSs. As shown in Fig. 3, the ZnO-NWs and MoS_2-NSs are uniformly coated on the fiber surface, increasing the attachment area of AuNPs and laying the groundwork for the excitation of the LSPR phenomenon, and the modification of NMs greatly improves the sensor's sensing performance.

The chosen NMs possess exceptional biocompatibility, facilitating the viability of active molecules. Additionally, their substantial specific surface area offers many sites for the attachment of AuNPs and biomolecules. Therefore, the immobilization of NMs plays a crucial role in determining the sensor's performance. Fig. 5(b)–(d) shows the HR-TEM images of the AuNPs, ZnO-NWs, and MoS_2-NSs NMs. The adhesion of NMs to the optical fiber can be examined using scanning electron microscopy. The ZnO-NWs exhibited a line-like irregular cross-distribution, while the MoS_2-NSs showed a lamellar stacking distribution. The nano-coating on the probe's surface formed a compact and uniform layer-like structure, indicating a well-distributed sensor. The probe surface's nano-coating, with its homogenous layer structure, provides a strong basis for the sensor's excellent sensing properties.

C. Measurement of RF Solutions

In this experiment, a series of five distinct concentrations of RF solutions were prepared. The LSPR spectra of the

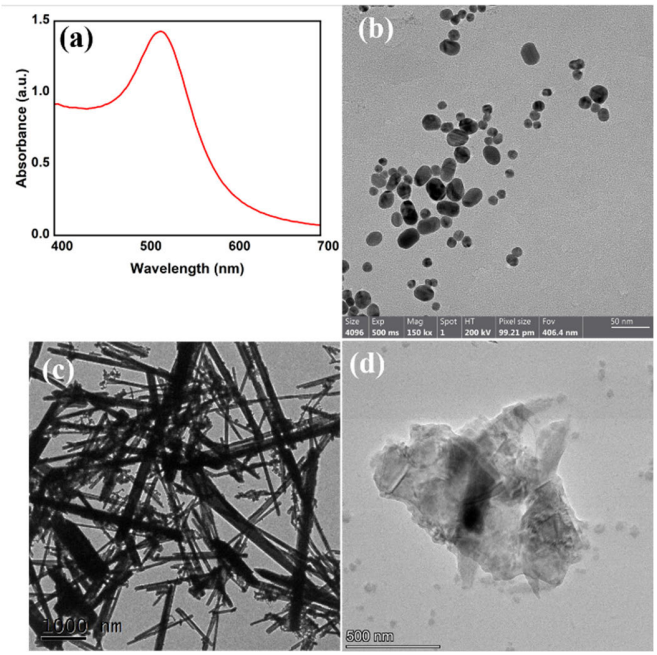

Fig. 5. (a) Absorbance spectrum of AuNPs, HR-TEM images of - (b) AuNPs, (c) ZnO-NWs, and (d) MoS_2-NSs.

RF sample solutions at various concentrations were evaluated using the sensor. The concentrations were measured in a sequential manner, ranging from 1 to 800 μM. Following each measurement, the probe and reaction cell were cleaned with PBS to avoid any interference between solutions of different concentrations. Subsequently, the probe and reaction cell were dried in preparation for the next measurement. The LSPR was then carried out using OSA, once the output spectra had stabilized, and the resulting data were recorded. To ensure the experiment's accuracy, the RF sample solutions were sequentially measured using three distinct probes, starting from low concentrations, and progressing to high concentrations. The LSPR spectra were adjusted to a standard scale to achieve normalization. Fig. 6(a) shows that the peak of the LSPR resonance spectrum shifts to the left as the concentration of the RF sample solution increases. This shift is caused by changes in the RF concentration around the probes, which in turn affects the EWs and leads to a change in the peak of the LSPR resonance spectrum. Fig. 6(b) displays the linear regression curve for the peak wavelength. The linear regression has a coefficient of determination of 0.99. The linear regression curve can be represented as

$$\lambda = 0.00214c + 1532.56 \quad (5)$$

where λ is the peak wavelength of the LSPR spectrum and c is the concentration of the RF solution. The LOD of the sensor can better reflect the sensing characteristics of the sensor, and the sensor developed in this work has an LOD = 86.86 μM.

D. Stability Test

The stability experiment is designed to determine whether the constructed sensor is stable, and that has a significant impact on the sensor's detection limit. OSA was used to

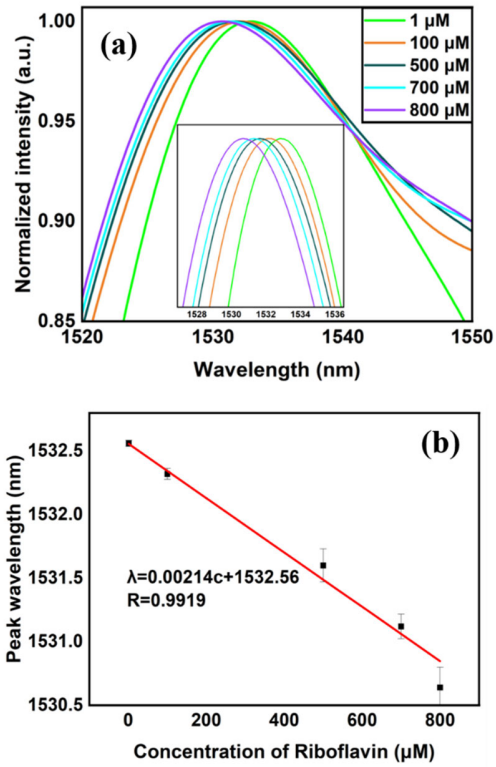

Fig. 6. Measurement of RF using the proposed TTIT-based fiber sensor (a) sensing spectrum and (b) linear plot of the proposed sensor.

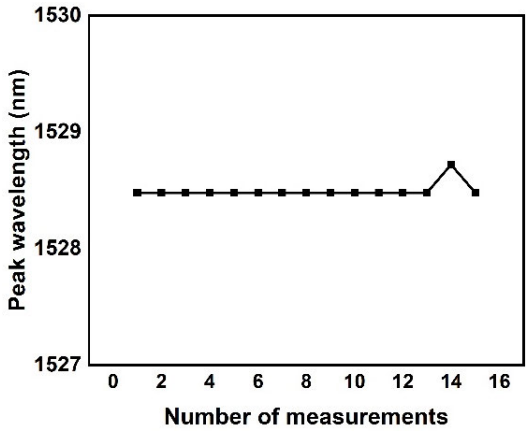

Fig. 7. Stability test of the developed sensor.

take fifteen similar measurements of the same probe in the same RF solution at an 800 μM concentration. The data were processed to extract the peak wavelength of each measurement. From Fig. 7, it is obvious that the developed sensor has good stability.

E. Reproducibility and Reusability Test

Reproducibility is an important factor in assessing the practicality of a technology. The performance of a sensor is closely tied to its ability to consistently produce accurate measurements of a target solution using probes developed through the same process. For this experiment, three probes were utilized to assess the consistency of 1000 μM RF samples within a controlled setting. It is important to rinse each sensor

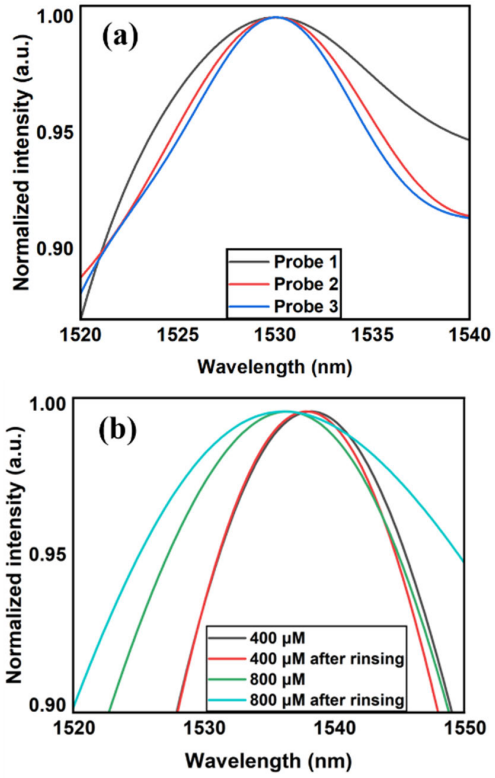

Fig. 8. (a) Reproducibility test and (b) reusability of the developed sensor.

probe with PBS before measurement to ensure the accuracy of the variables. The data analysis results are presented in Fig. 8(a), indicating the sensor's remarkable reproducibility during fabrication.

Testing the reusability of the sensor is crucial in determining its suitability for clinical application. For this experiment, solutions of RF with concentrations of 400 and 800 μM were chosen.

Two probes were chosen to measure sample solutions with concentrations of 400 and 800 μM. Each measurement required cleaning the probes with a PBS solution. The probes were left in the reaction cell for ten minutes. The data was then analyzed and plotted in Fig. 8(b). The results demonstrate that the sensor can be reused for the same concentration with excellent reproducibility.

F. Evaluation of Sensing Performance

In this study, a novel RF fiber-optic biosensor utilizing LSPR-based TTIT has been developed. Currently, there are various methods used both domestically and internationally to detect RF.

These methods include electrochemical detection, enzyme immunoassay, capillary electrophoresis, colorimetric detection, HPLC, fluorescence detection, mass spectrometry, and more. However, each of these methods has its own limitations. The most commonly used method for determining RF is HPLC, but this method is time-consuming and requires a large number of mobile phase solvents. Electrochemical methods are susceptible to interference, and fluorescence detection methods have a natural fluorescence response due to their own structure,

TABLE I
PERFORMANCE COMPARISON OF THE PROPOSED SENSOR WITH THE EXISTING RF SENSORS

Nano-materials used	Mechanisms	Linear range (μM)	Sensitivity	LoD	Ref.
ZnS/RGO	Electroanalytical analysis	0.3–1, 1–80	n.r.[a]	0.029 μM	[22]
AuNPs	Electroanalytical analysis	5 – 60	n.r.[a]	15.35 nM	[23]
$AgNO_3$	Versatile tri-modal	0–312.5	1.56 μA/mM/cm^2	2.5 μM	[24]
Carbon Dots	Fluorescence method	0-11	n.r.[a]	0.025 μM	[25]
MoS_2/MoO_3	Electroanalytical analysis	0-100	0.67 μA/μM	1.5 μM	[26]
AuNPs/ZnO/MoS_2	LSPR	1–800	2.14 nm/mM	86.86 μM	This work

[a]not reported

with many interfering factors, such as photodecomposition, oxygen quenching, and susceptibility to contamination. Fiber-optic biosensors offer exceptional sensing characteristics in comparison. Table I presents a comparison of the performance of different sensors. Table I revealed that the LSPR-based fiber optic biosensor offers a wider detection range, along with exceptional sensitivity and detection limits. This indicates that the sensors developed in this study can deliver precise data to fulfill the demands of measuring RF concentrations and can be effectively utilized, providing new alternatives for detecting RF concentrations.

IV. CONCLUSION

In this work, the authors developed a real-time, highly sensitive fiber-optic biosensor based on the MMF-SCF-MMF-based TTIT structure. The probe surface was coated with various NMs including AuNPs, ZnO-NWs, and MoS_2-NSs. The concentration of the target solution was measured by excitation of the LSPR phenomenon of AuNPs. The ZnO-NWs and MoS_2-NSs enhanced the attachment area of the fiber optic surface to increase the sensing area and improve the sensing characteristics of the sensor. It can be seen from the tests that the sensor developed in this work has higher sensitivity, high repeatability, and stability and has a wider range of measurement compared to other methods. The superior sensing characteristics of this sensor mean that the measured data are extremely accurate and can be put to use. This will advance the development of RF sensors and their use in the clinical field and food safety.

ACKNOWLEDGMENT

Ziyi Liu is with Ji Xianlin College and School of Physics Science and Information Technology, Liaocheng University, Liaocheng 252059, China (e-mail: 1003771607@qq.com).

Ragini Singh is with the Department of Biotechnology, Koneru Lakshmaiah Education Foundation, Vaddeswaram, Andhra Pradesh 522302, India (e-mail: raginisingh@kluniversity.in).

Guoju Wang, Guoru Li, and Bingyuan Zhang are with Shandong Key Laboratory of Optical Communication Science and Technology, School of Physics Science and Information Technology, Liaocheng University, Liaocheng 252059, China (e-mail: wangguoju@lcu.edu.cn; grli@lcu.edu.cn; zhangbingyuan@lcu.edu.cn).

Santosh Kumar is with Shandong Key Laboratory of Optical Communication Science and Technology, School of Physics Science and Information Technology, Liaocheng University, Liaocheng 252059, China, and also with the Centre of Excellence for Nanotechnology, Department of Electronics and Communication Engineering, Koneru Lakshmaiah Education Foundation, Vaddeswaram, Andhra Pradesh 522302, India (e-mail: santosh@kluniversity.in).

REFERENCES

[1] N. Olfat, M. Ashoori, and A. Saedisomeolia, "Riboflavin is an antioxidant: A review update," *Brit. J. Nutrition*, vol. 128, no. 10, pp. 1887–1895, Nov. 2022, doi: 10.1017/s0007114521005031.

[2] L. A. Averianova, L. A. Balabanova, O. M. Son, A. B. Podvolotskaya, and L. A. Tekutyeva, "Production of vitamin B2 (riboflavin) by microorganisms: An overview," *Frontiers Bioeng. Biotechnol.*, vol. 8, p. 2020, Nov. 2020, doi: 10.3389/fbioe.2020.570828.

[3] S. Mosegaard, G. Dipace, P. Bross, J. Carlsen, N. Gregersen, and R. K. J. Olsen, "Riboflavin deficiency—Implications for general human health and inborn errors of metabolism," *Int. J. Mol. Sci.*, vol. 21, no. 11, p. 3847, May 2020, doi: 10.3390/ijms21113847.

[4] D. Plantone, M. Pardini, and G. Rinaldi, "Riboflavin in neurological diseases: A narrative review," *Clin. Drug Invest.*, vol. 41, no. 6, pp. 513–527, Jun. 2021, doi: 10.1007/s40261-021-01038-1.

[5] S. Balasubramaniam, J. Christodoulou, and S. Rahman, "Disorders of riboflavin metabolism," *J. Inherited Metabolic Disease*, vol. 42, no. 4, pp. 608–619, Jul. 2019, doi: 10.1002/jimd.12058.

[6] S. Chelly, M. Chelly, R. Zribi, R. Gdoura, H. Bouaziz-Ketata, and G. Neri, "Electrochemical detection of dopamine and riboflavine on a screen-printed carbon electrode modified by AuNPs derived from *Rhanterium suaveolens* plant extract," *ACS Omega*, vol. 6, no. 37, pp. 23666–23675, Sep. 2021, doi: 10.1021/acsomega.1c00793.

[7] T. R. I. Cataldi, D. Nardiello, L. Scrano, and A. Scopa, "Assay of riboflavin in sample wines by capillary zone electrophoresis and laser-induced fluorescence detection," *J. Agricult. Food Chem.*, vol. 50, no. 23, pp. 6643–6647, Nov. 2002, doi: 10.1021/jf020212a.

[8] Z. Song et al., "Dual-mode detection of cysteamine using Ag nanoparticle-riboflavin composites," *ACS Appl. Nano Mater.*, vol. 7, no. 7, pp. 6995–7007, Apr. 2024, doi: 10.1021/acsanm.3c06074.

[9] L. Kang et al., "Rapid determination of folic acid and riboflavin in urine by polypyrrole magnetic solid-phase extractant combined ultra-performance liquid chromatography," *J. Chromatography A*, vol. 1648, Jul. 2021, Art. no. 462192, doi: 10.1016/j.chroma.2021.462192.

[10] P. Russo et al., "Selection of riboflavin overproducing strains of lactic acid bacteria and riboflavin direct quantification by fluorescence," in *Flavins and Flavoproteins*, vol. 2280, M. Barile, Ed., New York, NY, USA: Springer, 2021, doi: 10.1007/978-1-0716-1286-6_1.

[11] K. Porter and J. K. Lodge, "Determination of selected water-soluble vitamins (thiamine, riboflavin, nicotinamide and pyridoxine) from a food matrix using hydrophilic interaction liquid chromatography coupled with mass spectroscopy," *J. Chromatography B*, vol. 1171, May 2021, Art. no. 122541, doi: 10.1016/j.jchromb.2021.122541.

[12] M. Xie et al., "Going even smaller: Engineering sub-5 nm nanoparticles for improved delivery, biocompatibility, and functionality," *WIREs Nanomedicine Nanobiotechnology*, vol. 12, no. 6, p. e1644, Nov. 2020, doi: 10.1002/wnan.1644.

[13] N. Baig, I. Kammakakam, and W. Falath, "Nanomaterials: A review of synthesis methods, properties, recent progress, and challenges," *Mater. Adv.*, vol. 2, no. 6, pp. 1821–1871, 2021, doi: 10.1039/d0ma00807a.

[14] K. Nejati, M. Dadashpour, T. Gharibi, H. Mellatyar, and A. Akbarzadeh, "Biomedical applications of functionalized gold nanoparticles: A review," *J. Cluster Sci.*, vol. 33, no. 1, pp. 1–16, Jan. 2022, doi: 10.1007/s10876-020-01955-9.

[15] X. Bai et al., "The basic properties of gold nanoparticles and their applications in tumor diagnosis and treatment," *Int. J. Mol. Sci.*, vol. 21, no. 7, p. 2480, Apr. 2020, doi: 10.3390/ijms21072480.

[16] H.-M. Kim, J.-H. Park, and S.-K. Lee, "Fiber optic sensor based on ZnO nanowires decorated by Au nanoparticles for improved plasmonic biosensor," *Sci. Rep.*, vol. 9, no. 1, p. 15605, Oct. 2019, doi: 10.1038/s41598-019-52056-1.

[17] P. Feng, S. Shen, L. Yang, Y. Kong, S. Yang, and C. Shuai, "Vertical and uniform growth of MoS_2 nanosheets on GO nanosheets for efficient mechanical reinforcement in polymer scaffold," *Virtual Phys. Prototyping*, vol. 18, no. 1, Dec. 2023, Art. no. e2115384, doi: 10.1080/17452759.2022.2115384.

[18] H. Zhang, X. Zhou, X. Li, P. Gong, Y. Zhang, and Y. Zhao, "Recent advancements of LSPR fiber-optic biosensing: Combination methods, structure, and prospects," *Biosensors*, vol. 13, no. 3, p. 405, Mar. 2023, doi: 10.3390/bios13030405.

[19] G. Zhu et al., "Tapered optical fiber-based LSPR biosensor for ascorbic acid detection," *Photonic Sensors*, vol. 11, no. 4, pp. 418–434, Dec. 2021, doi: 10.1007/s13320-020-0605-2.

[20] J. Goicoechea, P. J. Rivero, S. Sada, and F. J. Arregui, "Self-referenced optical fiber sensor for hydrogen peroxide detection based on LSPR of metallic nanoparticles in layer-by-layer films," *Sensors*, vol. 19, no. 18, p. 3872, Sep. 2019, doi: 10.3390/s19183872.

[21] J. Turkevich, P. C. Stevenson, and J. Hillier, "A study of the nucleation and growth processes in the synthesis of colloidal gold," *Discuss. Faraday Soc.*, vol. 11, pp. 55–75, May 1951, doi: 10.1039/DF9511100055.

[22] W. Zhang, Y. Qiao, Q. Fan, N. Li, and J. Qiao, "Electrochemical detection of riboflavin by ZnS/RGO nanomaterial synthesized by microwave method," *J. Shanxi Agricult. Univ.*, vol. 46, no. 3, pp. 681–688, 2023, doi: 10.13451/j.sxu.ns.2022022.

[23] D. N. Varun et al., "Simple and sensitive electrochemical analysis of riboflavin at functionalized carbon nanofiber modified carbon nanotube sensor," *Monatshefte Für Chem.-Chem. Monthly*, vol. 152, no. 10, pp. 1183–1191, Oct. 2021, doi: 10.1007/s00706-021-02839-y.

[24] E. Priyadarshini, K. Rawat, and H. B. Bohidar, "Multimode sensing of riboflavin via Ag@carbon dot conjugates," *Appl. Nanosci.*, vol. 10, no. 1, pp. 281–291, Jan. 2020, doi: 10.1007/s13204-019-01090-6.

[25] R. Sotolongo-García, E. Rodríguez-Velázquez, M. Alatorre-Meda, M. T. Oropeza-Guzmán, A. Tirado-Guízar, and G. Pina-Luis, "Optimizing the efficiency of a cytocompatible carbon-dots-based FRET platform and its application as a riboflavin sensor in beverages," *Nanomaterials*, vol. 11, no. 8, p. 1981, Jul. 2021, doi: 10.3390/nano11081981.

[26] R. Zribi, A. Foti, M. G. Donato, P. G. Gucciardi, and G. Neri, "Fabrication of a novel electrochemical sensor based on carbon cloth matrix functionalized with MoO_3 and 2D-MoS_2 layers for riboflavin determination," *Sensors*, vol. 21, no. 4, p. 1371, Feb. 2021, doi: 10.3390/s21041371.